SCIENCE CHINA
Information Sciences

• RESEARCH PAPER •
October 2021, Vol. 64 200302:1–200302:15
https://doi.org/10.1007/s11432-021-3281-7
Special Focus on Reconfigurable Intelligent Surfaces for Future Wireless Communications

Low-cost intelligent reflecting surface aided Terahertz multiuser massive MIMO: design and analysis

Guanghua YU, Xiaoming CHEN*, Xiaodan SHAO & Caijun ZHONG

College of Information Science and Electronic Engineering, Zhejiang University, Hangzhou 310027*, China*

Received 4 March 2021/Revised 23 April 2021/Accepted 4 June 2021/Published online 7 September 2021

Abstract Terahertz (THz) multiuser massive multiple-input multiple-output (MIMO) has been envisioned as a promising technique to support massive connectivity in next-generation wireless networks. However, due to ultra-high frequency band, the path attenuation of THz channels is extremely severe, resulting in limited wireless coverage. In this paper, we propose an intelligent reflecting surface (IRS)-assisted THz multiuser massive MIMO technique to enhance coverage. First, we design an IRS-assisted THz communication framework with a low-cost sub-connected hybrid precoding architecture, including uplink data transmission and downlink data transmission. In particular, precoding errors due to the limitations of physical devices and environments are taken into consideration. Then, we derive the closed-form expressions for uplink and downlink spectral efficiencies, and reveal the impacts of system parameters. Finally, we conduct extensive simulations to verify the effectiveness of the proposed IRS-assisted THz multiuser massive MIMO technique.

Keywords THz communication, IRS, massive MIMO, precoding error, coverage enhancement.

Citation Yu G H, Chen X M, Shao X D, et al. Low-cost intelligent reflecting surface aided Terahertz multiuser massive MIMO: design and analysis. Sci China Inf Sci, 2021, 64(10): 200302, https://doi.org/10.1007/s11432-021-3281-7

1 Introduction

In the past few years, the widespread applications of Internet of Things (IoT) in various fields have greatly increased the demand for low power, massive connectivity, and wide coverage wireless networks [1–3]. As of 2020, the number of IoT devices has exceeded tens of billions [4, 5]. With the explosive growth of IoT devices, the future 6G wireless networks need to meet higher performance requirements, e.g., 1 Tbps peak data rates, 1 Gbps experienced data rates for users, 10–100 μs latency, 99.99999% reliability, and 10^7 devices/km^2 connectivity density [5, 6]. Although the use of advanced physical layer techniques, e.g., massive multiple-input multiple-output (MIMO) [7,8] and non-orthogonal multiple access (NOMA) [9,10], it is difficult to meet these requirements under the traditional bandwidth limitation. To tackle this problem preferably, it is time to break the frequency band constraints to explore new wireless communication solutions.

As an effective wideband communication technology, millimeter-wave (mmWave) communications (30–300 GHz) provide a larger frequency band range than traditional microwave communications [11, 12]. Although the peak rate in mmWave band can reach several Gbps, it is still not sufficient to meet the continuously increasing data traffic in 6G wireless networks [13]. Recently, Terahertz (THz) communications (0.1–10 THz) have attracted a great deal of attention from academia and industry [14]. THz communications can offer an unprecedented increment in the bandwidth, which makes it possible to support a much higher data rate compared with mmWave communications [15]. However, THz communication suffers from severe path attenuations, which originates from the ultra-high frequency. In [16–19], the THz channel particularities have been thoroughly investigated. Due to the free space attenuation, the molecular absorption loss, and adverse weather conditions experienced by THz wave, THz communication is greatly limited by the propagation distance. Although massive MIMO is employed in THz communications, wireless coverage is still unsatisfactory, especially at the edge of cells.

* Corresponding author (email: chen_xiaoming@zju.edu.cn)

To tackle this problem, intelligent reflecting surface (IRS) has been presented as a promising enabler. IRS has been proved to be able to significantly enhance the coverage of wireless communications [20–22]. Besides, IRS has the advantages of low hardware cost, low power consumption and simple structure, which makes it practical for THz communication assisted by IRS to realize and commercialize [23,24]. At present, the THz communication assisted by IRS has been extensively investigated in both academia and industry. In [25], a cooperative channel estimation procedure and transmission solutions were proposed for IRS-assisted THz communication systems. Then, a deep learning-based channel estimation (DL-CE) scheme was developed to solve the sparse recovery problem for THz communication systems assisted by IRS [26]. Moreover, an iterative atom pruning based subspace pursuit (IAP-SP) scheme was developed for channel estimation and a novel feed-forward fully connected structure-based deep neural network (DNN) scheme was proposed for performance optimization in [27]. Furthermore, the authors in [28] put forward a cross-entropy method that was feasible to promote the performance for IRS-assisted THz communication systems. In [29], the transmit beamforming at the base station (BS) and the reflecting matrix at the IRS were jointly optimized with transmit power and discrete phase-shift constraints to maximize the system secrecy rate.

Most previous studies consider the single-user scenarios. It is still lack of theoretical analysis and algorithm design for IRS-assisted THz massive MIMO systems in the multiuser scenarios. In this paper, we thoroughly investigate the performance of the designed IRS-assisted THz multiuser massive MIMO system and reveal the impact of system parameters on spectral efficiency. The main contributions can be summarized as follows:

(1) We design a framework with a low-cost sub-connected hybrid precoding architecture for IRS-assisted THz multiuser massive MIMO systems, including uplink and downlink data transmission. Considering physical limitations practically, precoding errors are taken into consideration.

(2) We analyze the performance of IRS-assisted THz multiuser massive MIMO systems and derives closed-form expressions for uplink and downlink spectral efficiencies. Then, the impacts of key system parameters are revealed.

The rest of this paper is organized as follows: Section 2 designs a framework for IRS-assisted THz multiuser massive MIMO system with sub-connected architecture and proposes the beamforming schemes at the BS and IRS. Then, Section 3 conducts performance analysis and derives closed-form expressions for uplink and downlink spectral efficiencies. Section 4 presents extensive simulations to verify the effectiveness of the proposed IRS-assisted THz multiuser massive MIMO technique. Finally, Section 5 concludes the paper.

Notations. We use bold upper (lower) letters to denote matrices (column vectors), $(\cdot)^{\mathrm{H}}$ to denote conjugate transpose, $\mathrm{E}[\cdot]$ to denote expectation, $\mathrm{var}(\cdot)$ to denote the variance, $\|\cdot\|$ to denote the L_2-norm of a vector and a matrix, $\mathrm{tr}(\cdot)$ to denote the trace of a matrix, $\otimes$ to denote the Kronecker product, $\odot$ to denote the product of the corresponding elements of the two matrices, $|\cdot|$ to denote the absolute value, and $\mathrm{Re}(\cdot)$ to denote the real part of a complex number, $\mathrm{diag}(a_1,\ldots,a_n)$ to denote the diagonal matrix with diagonal elements a_1, ..., and a_n, $\mathrm{diag}(\boldsymbol{A})$ to denote the diagonal matrix which only keep the diagonal elements of the matrix $\boldsymbol{A}$, $\mathrm{vec}(\mathrm{diag}(\boldsymbol{A}))$ to denote the column vector with respect to the diagonal elements of the matrix $\boldsymbol{A}$, $(\boldsymbol{A})_{i,j}$ to denote the (i,j)-th element of the matrix $\boldsymbol{A}$.

2 System model

We consider a THz multiuser massive MIMO system operated in a time division duplex mode (TDD), where a BS equipped with N_t antennas serves K single-antenna devices. For the sake of reducing the cost, a sub-connected architecture is adopted at the BS. Specifically, there are N_s radio frequency (RF) chains, each of which is connected to a nonoverlapping antenna sub-array with M antenna elements through a phase shifter network. Thus, we have $N_t = MN_s$. In this case, the number of required RF chains and the corresponding cost are decreased significantly. Since THz wave has the characteristics of high frequency and large propagation loss, it is reasonably assumed that the direct propagation paths between the BS and the devices are blocked, as shown in Figure 1. In order to enhance the coverage of THz massive MIMO, an IRS consisting of N_r reflecting units is employed to aid the communications between the BS and the devices. Without loss of generality, we focus on data transmission in a time slot, including uplink data transmission and downlink data transmission. Prior to discussing data transmission, we introduce the THz channel model.

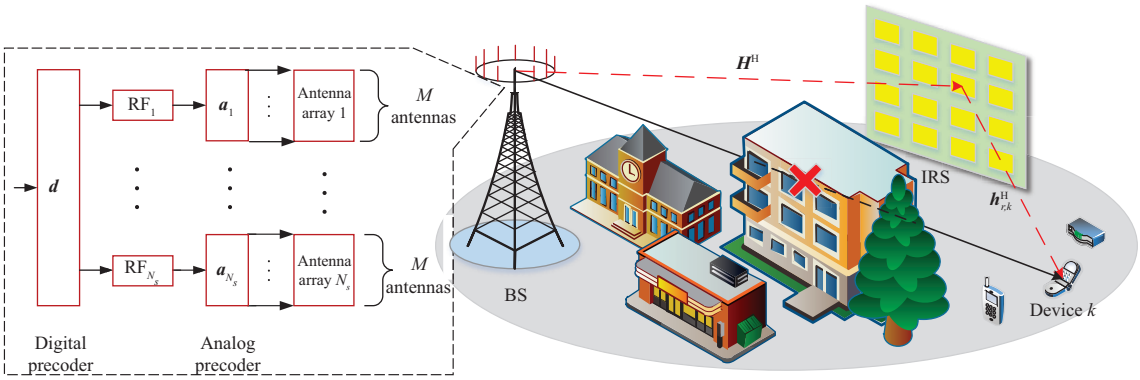

Figure 1 (Color online) Terahertz massive MIMO enhanced by an intelligent reflecting surface with a sub-connected architecture.

2.1 Channel model

According to the theory of electromagnetic wave propagation, THz channels usually contain a line-of-sight (LoS) component and a non-line-of-sight (NLoS) component [30, 31]. Thus, the channels from the BS to the IRS and from the IRS to the kth device can be expressed as

$$\boldsymbol{H} = \bar{\boldsymbol{H}} + \tilde{\boldsymbol{H}}, \tag{1}$$

and

$$\boldsymbol{h}_{r,k} = \bar{\boldsymbol{h}}_{r,k} + \tilde{\boldsymbol{h}}_{r,k}, \tag{2}$$

respectively, where $\bar{\boldsymbol{H}}$ and $\bar{\boldsymbol{h}}_{r,k}$ are the LoS component, $\tilde{\boldsymbol{H}}$ and $\tilde{\boldsymbol{h}}_{r,k}$ are the NLoS component. Since THz channels are expected to have limited scattering, we adopt geometric channel models with L scatterers between the BS and the IRS and L_k scatters between the IRS and the kth device. Assuming that each scatterer contributes a single propagation path, the THz channels can be rewritten as

$$\boldsymbol{H} = \alpha_{\mathrm{LoS}}\boldsymbol{a}(N_t, \phi^r_{\mathrm{LoS}}, \theta^r_{\mathrm{LoS}})\boldsymbol{a}^{\mathrm{H}}(N_r, \phi^t_{\mathrm{LoS}}, \theta^t_{\mathrm{LoS}}) + \sum_{l=1}^{L} \alpha_l \boldsymbol{a}(N_t, \phi^r_l, \theta^r_l)\boldsymbol{a}^{\mathrm{H}}(N_r, \phi^t_l, \theta^t_l), \tag{3}$$

and

$$\boldsymbol{h}_{r,k} = \beta_{\mathrm{LoS},k}\boldsymbol{a}(N_r, \phi^r_{\mathrm{LoS},k}, \theta^r_{\mathrm{LoS},k}) + \sum_{l=1}^{L_k} \beta_{l,k} \boldsymbol{a}(N_r, \phi^r_{l,k}, \theta^r_{l,k}), \tag{4}$$

where α_{LoS} and $\beta_{\mathrm{LoS},k}$ are the distance-dependent path loss. As discussed in [32, 33], the path loss α_{LoS} is given by

$$\alpha_{\mathrm{LoS}} = \alpha^{\mathrm{spr}}_{\mathrm{LoS}} \cdot \alpha^{\mathrm{abs}}_{\mathrm{LoS}}, \tag{5}$$

where $\alpha^{\mathrm{spr}}_{\mathrm{LoS}}$ and $\alpha^{\mathrm{abs}}_{\mathrm{LoS}}$ respectively consider the effect of spreading and molecular absorption loss and can be obtained as

$$\alpha^{\mathrm{spr}}_{\mathrm{LoS}} = \frac{\mathrm{c}}{4\pi f d_{\text{BS-IRS}}}, \tag{6}$$

and

$$\alpha^{\mathrm{abs}}_{\mathrm{LoS}} = \mathrm{e}^{-\frac{1}{2}k(f)d_{\text{BS-IRS}}}, \tag{7}$$

where c is the speed of light in vacuum, f is the center frequency, $d_{\text{BS-IRS}}$ is the distance from the BS to the IRS, $k(f)$ is the medium absorption coefficient. The parameter $\beta_{l,k}$ can be obtained in the similar way. α_l and $\beta_{l,k}$ are complex gains and follow the independent and identical distribution (i.i.d) $\alpha_l \sim N_c(0, \sigma^2_\alpha)$ and $\beta_{l,k} \sim N_c(0, \sigma^2_{\beta,k})$ with σ^2_α and $\sigma^2_{\beta,k}$ being the average power. Wherein, σ_α can be expressed as

$$\sigma_\alpha = c(f) \cdot \frac{\mathrm{c}}{4\pi f d_{\text{BS-IRS}}} \cdot \mathrm{e}^{-\frac{1}{2}k(f)d_{\text{BS-IRS}}}, \tag{8}$$

where $c(f)$ is the reflection coefficient. $\sigma_{\beta,k}$ can be constructed in the similar way. Besides, $\boldsymbol{a}(\cdot)$ is the antenna array response vectors. The variables $\phi^r_l(\theta^r_l) \in [0, 2\pi]$ and $\phi^t_l(\theta^t_l) \in [0, 2\pi]$ are the lth

path's azimuth angles of arrival and departure (AoAs/AODs) of the BS and the IRS respectively, and $\phi^r_{l,k}(\theta^r_{l,k}) \in [0, 2\pi]$ is the AoAs of the IRS for the kth device. $\phi^r_{\mathrm{LoS}}(\theta^r_{\mathrm{LoS}}) \in [0, 2\pi]$ and $\phi^t_{\mathrm{LoS}}(\theta^t_{\mathrm{LoS}}) \in [0, 2\pi]$ are the AoAs and AoDs of the LoS component, and $\phi^r_{\mathrm{LoS},k}(\theta^r_{\mathrm{LoS},k})$ is the AoAs of the LoS component. In the case of the uniform planar array (UPA) with W and H elements ($WH = N$) on horizon and vertical, respectively, the array response vector an be expressed as [34]

$$\boldsymbol{a}(N, \phi, \theta) = [1, \ldots, \mathrm{e}^{\mathrm{j}(2\pi/\lambda)d(x\sin(\phi)\sin(\theta)+y\cos(\theta))}, \ldots, \mathrm{e}^{\mathrm{j}(2\pi/\lambda)d((W-1)\sin(\phi)\sin(\theta)+(H-1)\cos(\theta))}]^{\mathrm{T}}, \tag{9}$$

with λ being the signal wavelength, d being the distance between antenna elements, $0 \leqslant x \leqslant (W-1)$ and $0 \leqslant y \leqslant (H-1)$.

For convenience, the NLoS components of the THz channels are rewritten as the following matrix form:

$$\tilde{\boldsymbol{H}} = \boldsymbol{A}_r \boldsymbol{\Lambda} \boldsymbol{A}_t^{\mathrm{H}}, \tag{10}$$

and

$$\tilde{\boldsymbol{h}}_{r,k} = \boldsymbol{A}_k \boldsymbol{v}_k, \tag{11}$$

where

$$\boldsymbol{\Lambda} = \mathrm{diag}[\alpha_1, \ldots, \alpha_L], \tag{12}$$

$$\boldsymbol{v}_k = [\beta_{1,k}, \ldots, \beta_{L_k,k}]^{\mathrm{T}}, \tag{13}$$

$$\boldsymbol{A}_r = [\boldsymbol{a}(N_t, \phi^r_1, \theta^r_1), \ldots, \boldsymbol{a}(N_t, \phi^r_L, \theta^r_L)], \tag{14}$$

$$\boldsymbol{A}_t = [\boldsymbol{a}(N_r, \phi^t_1, \theta^t_1), \ldots, \boldsymbol{a}(N_r, \phi^t_L, \theta^t_L)], \tag{15}$$

and

$$\boldsymbol{A}_k = [\boldsymbol{a}(N_r, \phi^r_{1,k}, \theta^r_{1,k}), \ldots, \boldsymbol{a}(N_r, \phi^r_{L_k,k}, \theta^r_{L_k,k})]. \tag{16}$$

Thus, the uplink channel $\boldsymbol{h}_k$ from the kth device to the BS can be modeled as

$$\begin{aligned} \boldsymbol{h}_k &= \boldsymbol{H}\boldsymbol{\Theta}\boldsymbol{h}_{r,k} \\ &= \bar{\boldsymbol{H}}\boldsymbol{\Theta}\bar{\boldsymbol{h}}_{r,k} + \bar{\boldsymbol{H}}\boldsymbol{\Theta}\tilde{\boldsymbol{h}}_{r,k} + \tilde{\boldsymbol{H}}\boldsymbol{\Theta}\bar{\boldsymbol{h}}_{r,k} + \tilde{\boldsymbol{H}}\boldsymbol{\Theta}\tilde{\boldsymbol{h}}_{r,k} \\ &= \bar{\boldsymbol{H}}\boldsymbol{\Theta}\bar{\boldsymbol{h}}_{r,k} + \bar{\boldsymbol{H}}\boldsymbol{\Theta}\boldsymbol{A}_k\boldsymbol{v}_k + \boldsymbol{A}_t\boldsymbol{\Lambda}\boldsymbol{A}_r^{\mathrm{H}}\boldsymbol{\Theta}\bar{\boldsymbol{h}}_{r,k} + \boldsymbol{A}_t\boldsymbol{\Lambda}\boldsymbol{A}_r^{\mathrm{H}}\boldsymbol{\Theta}\boldsymbol{A}_k\boldsymbol{v}_k, \end{aligned} \tag{17}$$

where $\boldsymbol{\Theta}$ represents the diagonal phase-shifting matrix of the IRS. To strike a balance between the performance and the computation in a multiuser massive MIMO system, $\boldsymbol{\Theta}$ is designed based on the weighted array of all devices' channels, which is given by

$$\boldsymbol{\Theta} = \eta\mathrm{diag}\left(\frac{\sum_{i=1}^{K}\sqrt{\rho_i}\boldsymbol{h}_{r,i}^{\mathrm{H}}}{\sqrt{\sum_{i=1}^{K}\rho_i\mathrm{E}[\|\boldsymbol{h}_{r,i}\|^2]}}\right) \tag{18}$$

with $\eta \in [0, 1]$ being the amplitude reflection coefficient and ρ_i being the weight factor for the ith device. The weighted factor determines the priority of the corresponding device. As shown in (18), the design of $\boldsymbol{\Theta}$ considers the channels of all devices comprehensively, which makes it possible to improve the overall performance.

2.2 Uplink data transmission

During the phase of uplink data transmission, the devices send signals to the BS simultaneously. The received signal $\boldsymbol{y}^u$ can be written as

$$\boldsymbol{y}^u = \sum_{k=1}^{K}\sqrt{P_k^u}\boldsymbol{h}_k s_k^u + \boldsymbol{n}, \tag{19}$$

where P_k^u is the uplink data transmit power, s_k^u is the complex Gaussian distributed data signal, and $\boldsymbol{n}$ is additive white Gaussian noise (AWGN) with variance σ_u^2. By applying the sub-connected hybrid decoding architecture, the post-decoding signal can be written as

$$y_k^u = (\boldsymbol{\Gamma}_k\boldsymbol{d}_k)^{\mathrm{H}}\boldsymbol{y}^u$$

$$= (\boldsymbol{\Gamma}_k \boldsymbol{d}_k)^{\mathrm{H}} \left(\sum_{i=1}^{K} \sqrt{P_i^u} \boldsymbol{h}_i s_i^u + \boldsymbol{n} \right)$$

$$= \sqrt{P_k^u} (\boldsymbol{\Gamma}_k \boldsymbol{d}_k)^{\mathrm{H}} \boldsymbol{h}_k s_k^u + \sum_{i=1, i \neq k}^{K} \sqrt{P_i^u} (\boldsymbol{\Gamma}_k \boldsymbol{d}_k)^{\mathrm{H}} \boldsymbol{h}_i s_i^u + (\boldsymbol{\Gamma}_k \boldsymbol{d}_k)^{\mathrm{H}} \boldsymbol{n}, \tag{20}$$

where $\boldsymbol{\Gamma}_k \in \mathcal{C}^{N_t \times N_s}$ is given by

$$\boldsymbol{\Gamma}_k = \begin{bmatrix} \boldsymbol{a}_{1,k} & \boldsymbol{0} & \cdots & \boldsymbol{0} \\ \boldsymbol{0} & \boldsymbol{a}_{2,k} & \cdots & \boldsymbol{0} \\ \vdots & \vdots & \ddots & \vdots \\ \boldsymbol{0} & \boldsymbol{0} & \cdots & \boldsymbol{a}_{N_s,k} \end{bmatrix}, \tag{21}$$

with $\boldsymbol{a}_{n,k} \in \mathcal{C}^{M \times 1}$ being the analog decoder. Notice that the elements of $\boldsymbol{a}_{n,k}$ have the same amplitude $1/\sqrt{M}$ but different phases [35]. To achieve a balance between the system performance and computation complexity, we adopt maximum ratio combination (MRC) to decrease the inter-device interference. MRC is commonly used in multiuser massive MIMO due to its simplicity and effectiveness [36]. Equivalently, the digital decoder for the kth device's signal is designed as

$$\boldsymbol{d}_k = \frac{\boldsymbol{\Gamma}_k^{\mathrm{H}} \boldsymbol{h}_k}{\sqrt{\mathrm{E}[\|\boldsymbol{\Gamma}_k^{\mathrm{H}} \boldsymbol{h}_k\|^2]}}. \tag{22}$$

As for the analog decoder, we set it as a phase matcher for the corresponding channel. Mathematically, $\boldsymbol{a}_{n,k}$ can be expressed as

$$\boldsymbol{a}_{n,k} = \frac{\boldsymbol{h}_{n,k}}{\sqrt{\mathrm{E}[\|\boldsymbol{h}_{n,k}\|^2]}}, \tag{23}$$

where $\boldsymbol{h}_{n,k}$ is the channel vector with respect to the data stream over nth RF chain and we have

$$\boldsymbol{h}_k = [\boldsymbol{h}_{1,k}^{\mathrm{H}}, \ldots, \boldsymbol{h}_{n,k}^{\mathrm{H}}, \ldots, \boldsymbol{h}_{N_s,k}^{\mathrm{H}}]^{\mathrm{H}}. \tag{24}$$

Note that in the scenario of massive MIMO, the randomness of channel fading vanishes, namely channel hardening [37, 38]. In this case, the mean of channel vector is equivalent to the instantaneous channel vector. Hence, the amplitude of the analog decoder vector is unit.

As mentioned above, a low-cost sub-connected architecture is deployed for the multiuser THz massive MIMO system, where each radio frequency chain is connected to a non-overlapping antenna subarray through a phase shifter network. Due to environment and device factors, the value of a phase shifter may be changed, resulting in the phase shifter error. Consequently, the decoder designed based on the ideal phase shifter is erroneous. Taking phase error and gain error into consideration, the practically analog decoding matrix $\boldsymbol{\Gamma}_{k,e}$ can be expressed as

$$\boldsymbol{\Gamma}_{k,e} = \boldsymbol{\Delta}\boldsymbol{\Gamma}_k = \begin{bmatrix} \boldsymbol{\Delta}_1 \boldsymbol{a}_{1,k} & \boldsymbol{0} & \cdots & \boldsymbol{0} \\ \boldsymbol{0} & \boldsymbol{\Delta}_2 \boldsymbol{a}_{2,k} & \cdots & \vdots \\ \vdots & \vdots & \ddots & \boldsymbol{0} \\ \boldsymbol{0} & \cdots & \boldsymbol{0} & \boldsymbol{\Delta}_{N_s} \boldsymbol{a}_{N_s,k} \end{bmatrix} \tag{25}$$

with

$$\boldsymbol{\Delta}_m = \mathrm{diag}(\mu_{m,1} \mathrm{e}^{\mathrm{j}\nu_{m,1}}, \ldots, \mu_{m,M} \mathrm{e}^{\mathrm{j}\nu_{m,M}}), \tag{26}$$

where $\boldsymbol{\Delta} \in \mathcal{C}^{N_t \times N_t}$ denotes the analog decoding error matrix, $\mu_{m,n} \sim \mathcal{N}(1, \sigma_\mu^2)$ denotes the gain error, and $\nu_{m,n} \sim \mathcal{N}(0, \sigma_\nu^2)$ denotes the phase-shifting error[1)].

1) The analog decoding error is determined by the physical characteristics of the BS equipments and is independent of the channel vector and environmental noise. In addition, we assume that each element in $\boldsymbol{\Delta}$ is independent of each other.

Hence, the decoded signal can be written as

$$y_{k,e}^{u} = \sqrt{P_k^u}(\boldsymbol{\Gamma}_{k,e}\boldsymbol{d}_k)^{\mathrm{H}}\boldsymbol{h}_k s_k^u + \sum_{i=1,i\neq k}^{K} \sqrt{P_i^u}(\boldsymbol{\Gamma}_{k,e}\boldsymbol{d}_k)^{\mathrm{H}}\boldsymbol{h}_i s_i^u + (\boldsymbol{\Gamma}_{k,e}\boldsymbol{d}_k)^{\mathrm{H}}\boldsymbol{n}. \tag{27}$$

As shown in (27), the analog decoding error affects the expected signal, interference, and noise, resulting in performance loss.

2.3 Downlink data transmission

During the phase of downlink data transmission, the BS constructs a total transmission signal for all devices based on the sub-connected hybrid precoding architecture as follows:

$$\boldsymbol{x} = \sum_{k=1}^{K}(\boldsymbol{\Gamma}_k\boldsymbol{d}_k)\sqrt{P_k^d}s_k^d, \tag{28}$$

where P_k^d and s_k^d are the transmit power and the complex Gaussian distributed data signal for the kth device, respectively. Similarly, considering the phase-shifting error and gain error, the practically transmit signal can be rewritten as

$$\boldsymbol{x}_e = \sum_{k=1}^{K}(\boldsymbol{\Gamma}_{k,e}\boldsymbol{d}_k)\sqrt{P_k^d}s_k^d. \tag{29}$$

Note that $\boldsymbol{d}_k$ and $\boldsymbol{\Gamma}_{k,e}$ are designed as (22) and (25) due to channel reciprocity in the TDD mode. Then, the received signal at the kth device is given by

$$y_{k,e}^{d} = \sqrt{P_k^d}\boldsymbol{h}_k^{\mathrm{H}}(\boldsymbol{\Gamma}_{k,e}\boldsymbol{d}_k)s_k^d + \sum_{i=1,i\neq k}^{K} \sqrt{P_i^d}\boldsymbol{h}_k^{\mathrm{H}}(\boldsymbol{\Gamma}_{i,e}\boldsymbol{d}_i)s_i^d + n_k, \tag{30}$$

where n_k is AWGN with variance σ_d^2.

To reveal the impact of phase-shifting error and the function of IRS in THz multiuser massive MIMO, we conduct performance analysis in Section 3.

3 Performance analysis

In this section, with the goal of revealing the impact of the phase-shift error caused by the physical environment and the role of the IRS in coverage enhancement, we analyze the spectral efficiency of the IRS aided THz multiuser massive MIMO system.

3.1 Uplink (UL) spectral efficiency

Without loss of generality, we focus on the analysis of the spectral efficiency for the kth device over the uplink channel, which can be computed as

$$R_k^u = \mathrm{E}[\log_2(1+\gamma_k^u)], \tag{31}$$

where γ_k^u is the received signal-interference-plus-noise ratio (SINR) for the kth device and is given by

$$\gamma_k^u = \frac{P_k^u|(\boldsymbol{\Gamma}_{k,e}\boldsymbol{d}_k)^{\mathrm{H}}\boldsymbol{h}_k|^2}{\sum_{i=1,i\neq k}^{K} P_i^u|(\boldsymbol{\Gamma}_{k,e}\boldsymbol{d}_k)^{\mathrm{H}}\boldsymbol{h}_i|^2 + |(\boldsymbol{\Gamma}_{k,e}\boldsymbol{d}_k)^{\mathrm{H}}\boldsymbol{n}|^2}. \tag{32}$$

Note that the computation of the expectation with respect to a complicated random variable γ_k^u in (32) is not a trivial task. As a compromise, we turn to the derivation of a lower bound on the spectral efficiency, which is given by [37]

$$R_k^u \geqslant \underline{R}_k^u = \log_2(1+\underline{\gamma}_k^u), \tag{33}$$

where $\underline{\gamma}_k^u$ is the effective SINR and can be expressed as

$$\underline{\gamma}_k^u = \frac{\varpi_{0,k}^u}{\varpi_{1,k}^u + \varpi_{2,k}^u + \varpi_{3,k}^u} \tag{34}$$

with

$$\varpi_{0,k}^u = P_k^u |\mathrm{E}[(\boldsymbol{\Gamma}_{k,e}\boldsymbol{d}_k)^{\mathrm{H}}\boldsymbol{h}_k]|^2, \tag{35}$$

$$\varpi_{1,k}^u = P_k^u (\mathrm{E}[|(\boldsymbol{\Gamma}_{k,e}\boldsymbol{d}_k)^{\mathrm{H}}\boldsymbol{h}_k|^2] - |\mathrm{E}[(\boldsymbol{\Gamma}_{k,e}\boldsymbol{d}_k)^{\mathrm{H}}\boldsymbol{h}_k]|^2), \tag{36}$$

$$\varpi_{2,k}^u = \sum_{i=1, i\neq k}^{K} P_i^u \mathrm{E}[|(\boldsymbol{\Gamma}_{k,e}\boldsymbol{d}_k)^{\mathrm{H}}\boldsymbol{h}_i|^2], \tag{37}$$

and

$$\varpi_{3,k}^u = \mathrm{E}[|(\boldsymbol{\Gamma}_{k,e}\boldsymbol{d}_k)^{\mathrm{H}}\boldsymbol{n}|^2] \tag{38}$$

being the variances of the desired signal, the signal leakage, the residual inter-device interference, and the noise. These expectation terms can be computed as

$$\mathrm{E}[(\boldsymbol{\Gamma}_{k,e}\boldsymbol{d}_k)^{\mathrm{H}}\boldsymbol{h}_k] = \frac{\mathrm{E}[(\boldsymbol{\Gamma}_k^{\mathrm{H}}\boldsymbol{h}_k)^{\mathrm{H}}\boldsymbol{\Gamma}_{k,e}^{\mathrm{H}}\boldsymbol{h}_k]}{\sqrt{\mathrm{E}[\|\boldsymbol{\Gamma}_k^{\mathrm{H}}\boldsymbol{h}_k\|^2]}}, \tag{39}$$

$$\mathrm{E}[\|\boldsymbol{\Gamma}_k^{\mathrm{H}}\boldsymbol{h}_k\|^2] = \mathrm{tr}(\boldsymbol{R}_k\boldsymbol{R}_k^{\mathrm{sub}}), \tag{40}$$

$$\mathrm{E}[\|\boldsymbol{\Gamma}_k^{\mathrm{H}}\boldsymbol{h}_k\|^2] = |\mathrm{E}[(\bar{\boldsymbol{\Gamma}}_k^{\mathrm{H}} + \tilde{\boldsymbol{\Gamma}}_k^{\mathrm{H}})(\bar{\boldsymbol{h}}_k + \tilde{\boldsymbol{h}}_k)]|^2, \tag{41}$$

$$\mathrm{E}[(\boldsymbol{\Gamma}_k^{\mathrm{H}}\boldsymbol{h}_k)^{\mathrm{H}}\boldsymbol{\Gamma}_{k,e}^{\mathrm{H}}\boldsymbol{h}_k] = \mathrm{e}^{-\frac{\sigma_\nu^2}{2}}\mathrm{tr}(\boldsymbol{R}_k\boldsymbol{R}_k^{\mathrm{sub}}), \tag{42}$$

$$\mathrm{E}[|(\boldsymbol{\Gamma}_k^{\mathrm{H}}\boldsymbol{h}_k)^{\mathrm{H}}\boldsymbol{\Gamma}_{k,e}^{\mathrm{H}}\boldsymbol{h}_k|^2] = \mathrm{e}^{-\sigma_\nu^2}|\mathrm{tr}(\boldsymbol{R}_k\boldsymbol{R}_k^{\mathrm{sub}})|^2, \tag{43}$$

$$\mathrm{E}[|(\boldsymbol{\Gamma}_{k,e}\boldsymbol{d}_k)^{\mathrm{H}}\boldsymbol{h}_i|^2] = \frac{\mathrm{E}[|(\boldsymbol{\Gamma}_k^{\mathrm{H}}\boldsymbol{h}_k)^{\mathrm{H}}\boldsymbol{\Gamma}_{k,e}^{\mathrm{H}}\boldsymbol{h}_i|^2]}{\sqrt{\mathrm{E}[\|\boldsymbol{\Gamma}_k^{\mathrm{H}}\boldsymbol{h}_k\|^2]}}, \tag{44}$$

$$\mathrm{E}[|(\boldsymbol{\Gamma}_k^{\mathrm{H}}\boldsymbol{h}_k)^{\mathrm{H}}\boldsymbol{\Gamma}_{k,e}^{\mathrm{H}}\boldsymbol{h}_i|^2] = \mathrm{tr}(\boldsymbol{R}_k\boldsymbol{R}_k^{\mathrm{sub}}\boldsymbol{R}_i^e\boldsymbol{R}_k^{\mathrm{sub}}), \tag{45}$$

$$\mathrm{E}[|(\boldsymbol{\Gamma}_{k,e}\boldsymbol{d}_k)^{\mathrm{H}}\boldsymbol{n}|^2] = \frac{\mathrm{E}[|(\boldsymbol{\Gamma}_k^{\mathrm{H}}\boldsymbol{h}_k)^{\mathrm{H}}\boldsymbol{\Gamma}_{k,e}^{\mathrm{H}}\boldsymbol{n}|^2]}{\mathrm{E}[\|\boldsymbol{\Gamma}_k^{\mathrm{H}}\boldsymbol{h}_k\|^2]}, \tag{46}$$

and

$$\mathrm{E}[|(\boldsymbol{\Gamma}_k^{\mathrm{H}}\boldsymbol{h}_k)^{\mathrm{H}}\boldsymbol{\Gamma}_{k,e}^{\mathrm{H}}\boldsymbol{n}|^2] = \sigma_u^2(\sigma_\mu^2+1)\mathrm{tr}(\boldsymbol{R}_k\boldsymbol{R}_k^{\mathrm{sub}}\boldsymbol{R}_k^{\mathrm{sub}}), \tag{47}$$

where the autocorrelation matrix $\boldsymbol{R}_k$ of $\boldsymbol{h}_k$ is given by

$$\begin{aligned}
\boldsymbol{R}_{r,k} =\ & \bar{\boldsymbol{H}}\bar{\boldsymbol{\Theta}}\boldsymbol{R}_{r,k}\bar{\boldsymbol{\Theta}}^{\mathrm{H}}\bar{\boldsymbol{H}}^{\mathrm{H}} + \sigma_\alpha^2\boldsymbol{A}_r\mathrm{diag}(\boldsymbol{A}_t^{\mathrm{H}}\bar{\boldsymbol{\Theta}}\boldsymbol{R}_{r,k}\bar{\boldsymbol{\Theta}}^{\mathrm{H}}\boldsymbol{A}_t)\boldsymbol{A}_r^{\mathrm{H}} \\
& +2\mathrm{Re}\Bigg\{\frac{\eta\sqrt{\rho_k}}{\sqrt{\sum_{i=1}^K\rho_i\mathrm{tr}(\boldsymbol{R}_{r,i})}}(\bar{\boldsymbol{H}}\bar{\boldsymbol{\Theta}}\bar{\boldsymbol{h}}_{r,k}\mathrm{vec}(\mathrm{diag}(\boldsymbol{R}_{r,k}-\bar{\boldsymbol{h}}_{r,k}\bar{\boldsymbol{h}}_{r,k}^{\mathrm{H}}))^{\mathrm{T}}\bar{\boldsymbol{H}}^{\mathrm{H}} \\
& +\sigma_\alpha^2\boldsymbol{A}_r\mathrm{diag}(\boldsymbol{A}_t^{\mathrm{H}}\bar{\boldsymbol{\Theta}}\bar{\boldsymbol{h}}_{r,k}\mathrm{vec}(\mathrm{diag}(\boldsymbol{R}_{r,k}-\bar{\boldsymbol{h}}_{r,k}\bar{\boldsymbol{h}}_{r,k}^{\mathrm{H}}))^{\mathrm{T}}\boldsymbol{A}_t)\boldsymbol{A}_r^{\mathrm{H}} \\
& +\bar{\boldsymbol{H}}\bar{\boldsymbol{\Theta}}(\boldsymbol{R}_{r,k}-\bar{\boldsymbol{h}}_{r,k}\bar{\boldsymbol{h}}_{r,k}^{\mathrm{H}})\mathrm{diag}(\bar{\boldsymbol{h}}_{r,k}^{\mathrm{H}})\bar{\boldsymbol{H}}^{\mathrm{H}} \\
& +\sigma_\alpha^2\boldsymbol{A}_r\mathrm{diag}(\boldsymbol{A}_t^{\mathrm{H}}\bar{\boldsymbol{\Theta}}(\boldsymbol{R}_{r,k}-\bar{\boldsymbol{h}}_{r,k}\bar{\boldsymbol{h}}_{r,k}^{\mathrm{H}})\mathrm{diag}(\bar{\boldsymbol{h}}_{r,k}^{\mathrm{H}})\boldsymbol{A}_t)\boldsymbol{A}_r^{\mathrm{H}})\Bigg\} \\
& +\frac{\eta^2}{\sum_{i=1}^K\rho_i\mathrm{tr}(\boldsymbol{R}_{r,i})}\Bigg(\bar{\boldsymbol{H}}((\boldsymbol{R}_{r,i}-\bar{\boldsymbol{h}}_{r,i}\bar{\boldsymbol{h}}_{r,i}^{\mathrm{H}})\odot\boldsymbol{R}_{r,k})\bar{\boldsymbol{H}}^{\mathrm{H}} \\
& +\sum_{i=1}^K\rho_i\sigma_\alpha^2\boldsymbol{A}_r\mathrm{diag}(\boldsymbol{A}_t^{\mathrm{H}}((\boldsymbol{R}_{r,i}-\bar{\boldsymbol{h}}_{r,i}\bar{\boldsymbol{h}}_{r,i}^{\mathrm{H}})\odot\boldsymbol{R}_{r,k})\boldsymbol{A}_t)\boldsymbol{A}_r^{\mathrm{H}}\Bigg),
\end{aligned} \tag{48}$$

and $\boldsymbol{R}_k^{\text{sub}}$ can be expressed as

$$\boldsymbol{R}_k^{\text{sub}} = \begin{bmatrix} \dfrac{\boldsymbol{R}_{1,k}}{\text{tr}(\boldsymbol{R}_{1,k})} & \cdots & \boldsymbol{0} \\ \vdots & \ddots & \vdots \\ \boldsymbol{0} & \cdots & \dfrac{\boldsymbol{R}_{N_s,k}}{\text{tr}(\boldsymbol{R}_{N_s,k})} \end{bmatrix}. \tag{49}$$

$\boldsymbol{R}_{n,k}(n \in [1, N_s])$ is the autocorrelation matrix of $\boldsymbol{h}_{n,k}$, named $\boldsymbol{R}_{n,k} = \text{E}[\boldsymbol{h}_{n,k}\boldsymbol{h}_{n,k}^{\text{H}}]$. $\boldsymbol{R}_i^e$ is the autocorrelation matrix with respect to the precoding error and can be given by

$$(\boldsymbol{R}_i^e)_{m,n} = \begin{cases} (1+\sigma_\mu^2)(\boldsymbol{R}_i)_{m,n}, & m = n, \\ \text{e}^{-\sigma_v^2}(\boldsymbol{R}_i)_{m,n}, & m \neq n. \end{cases} \tag{50}$$

Proof. Please refer to Appendix C.

Combining (33)–(47), an approximated lower bound on the uplink spectral efficiency for the kth device can be obtained as

$$\underline{R}_k^u \approx \log_2\left(1 + \frac{P_k^u \text{e}^{-\sigma_\nu^2}|\text{tr}(\boldsymbol{R}_k\boldsymbol{R}_k^{\text{sub}})|^2}{\sum_{i=1,i\neq k}^K P_i^u \text{tr}(\boldsymbol{R}_k\boldsymbol{R}_k^{\text{sub}}\boldsymbol{R}_i^e\boldsymbol{R}_k^{\text{sub}}) + \sigma_u^2(\sigma_\mu^2+1)\text{tr}(\boldsymbol{R}_k\boldsymbol{R}_k^{\text{sub}}\boldsymbol{R}_k^{\text{sub}})}\right). \tag{51}$$

As can be seen in (51), the spectral efficiency is a decreasing function with respect to σ_μ and σ_ν, which means that eliminating the analog precoding error can significantly improve the performance of IRS-assisted THz multiuser massive MIMO systems.

3.2 Downlink (DL) spectral efficiency

As for the downlink data transmission, we also focus on the spectral efficiency of the kth device, which can be expressed as

$$R_k^d = \text{E}[\log_2(1+\gamma_k^d)], \tag{52}$$

where γ_k^d is the received SINR of the kth device, which is given by

$$\gamma_k^d = \frac{P_k^d|\boldsymbol{h}_k^{\text{H}}(\boldsymbol{\Gamma}_{k,e}\boldsymbol{d}_k)|^2}{\sum_{i=1,i\neq k}^K P_i^d|\boldsymbol{h}_k^{\text{H}}(\boldsymbol{\Gamma}_{i,e}\boldsymbol{d}_i)|^2 + \sigma_d^2}. \tag{53}$$

Similarly, we turn to the derivation of a lower bound on the spectral efficiency, which can be expressed as follows:

$$R_k^d \geqslant \underline{R}_k^d = \log_2(1+\underline{\gamma}_k^d), \tag{54}$$

where $\underline{\gamma}_k^d$ is the effective SINR and can be expressed as

$$\underline{\gamma}_k^d = \frac{\varpi_{0,k}^d}{\varpi_{1,k}^d + \varpi_{2,k}^d + \sigma_d^2} \tag{55}$$

with

$$\varpi_{0,k}^d = P_k^d|\text{E}[\boldsymbol{h}_k^{\text{H}}(\boldsymbol{\Gamma}_{k,e}\boldsymbol{d}_k)]|^2, \tag{56}$$

$$\varpi_{1,k}^d = P_k^d(\text{E}[|\boldsymbol{h}_k^{\text{H}}(\boldsymbol{\Gamma}_{k,e}\boldsymbol{d}_k)|^2] - |\text{E}[\boldsymbol{h}_k^{\text{H}}(\boldsymbol{\Gamma}_{k,e}\boldsymbol{d}_k)]|^2), \tag{57}$$

and

$$\varpi_{2,k}^d = \sum_{i=1,i\neq k}^K P_i^d\text{E}[|\boldsymbol{h}_k^{\text{H}}(\boldsymbol{\Gamma}_{i,e}\boldsymbol{d}_i)|^2]. \tag{58}$$

These expectation terms can be computed as

$$\text{E}[\boldsymbol{h}_k^{\text{H}}(\boldsymbol{\Gamma}_{k,e}\boldsymbol{d}_k)] = \frac{1}{\sqrt{\text{E}[\|\boldsymbol{\Gamma}_k^{\text{H}}\boldsymbol{h}_k\|^2]}}\text{E}[\boldsymbol{h}_k^{\text{H}}\boldsymbol{\Gamma}_{k,e}\boldsymbol{\Gamma}_k^{\text{H}}\boldsymbol{h}_k], \tag{59}$$

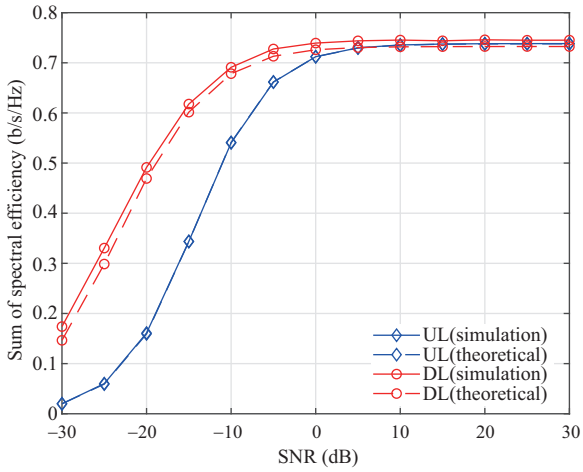

Figure 2 (Color online) Comparison of theoretical expressions and simulation results.

$$\mathrm{E}[\|\boldsymbol{\Gamma}_k^{\mathrm{H}}\boldsymbol{h}_k\|^2] = \mathrm{tr}(\boldsymbol{R}_k\boldsymbol{R}_k^{\mathrm{sub}}), \tag{60}$$

$$\mathrm{E}[\boldsymbol{h}_k\boldsymbol{\Gamma}_{k,e}\boldsymbol{\Gamma}_k^{\mathrm{H}}\boldsymbol{h}_k] = \mathrm{e}^{-\frac{\sigma_\nu^2}{2}}\mathrm{tr}(\boldsymbol{R}_k\boldsymbol{R}_k^{\mathrm{sub}}), \tag{61}$$

$$\mathrm{E}[\|\boldsymbol{h}_k^{\mathrm{H}}(\boldsymbol{\Gamma}_{k,e}\boldsymbol{d}_k)\|^2] = \frac{1}{\mathrm{E}[\|\boldsymbol{\Gamma}_k^{\mathrm{H}}\boldsymbol{h}_k\|^2]}\mathrm{E}[|\boldsymbol{h}_k^{\mathrm{H}}\boldsymbol{\Gamma}_{k,e}\boldsymbol{\Gamma}_k^{\mathrm{H}}\boldsymbol{h}_k|^2], \tag{62}$$

$$\mathrm{E}[|\boldsymbol{h}_k^{\mathrm{H}}\boldsymbol{\Gamma}_{k,e}\boldsymbol{\Gamma}_k^{\mathrm{H}}\boldsymbol{h}_k|^2] = \mathrm{e}^{-\sigma_\nu^2}|\mathrm{tr}(\boldsymbol{R}_k\boldsymbol{R}_k^{\mathrm{sub}})|^2, \tag{63}$$

$$\mathrm{E}[|\boldsymbol{h}_k^{\mathrm{H}}\boldsymbol{\Gamma}_{i,e}\boldsymbol{d}_i|^2] = \frac{1}{\mathrm{E}[\|\boldsymbol{\Gamma}_i^{\mathrm{H}}\boldsymbol{h}_i\|^2]}\mathrm{E}[|\boldsymbol{h}_k\boldsymbol{\Gamma}_{i,e}\boldsymbol{\Gamma}_i^{\mathrm{H}}\boldsymbol{h}_i|^2], \tag{64}$$

and

$$\mathrm{E}[|\boldsymbol{h}_k^{\mathrm{H}}\boldsymbol{\Gamma}_{i,e}\boldsymbol{\Gamma}_i^{\mathrm{H}}\boldsymbol{h}_i|^2] = \mathrm{tr}(\boldsymbol{R}_i\boldsymbol{R}_i^{\mathrm{sub}}\boldsymbol{R}_k^{e}\boldsymbol{R}_i^{\mathrm{sub}}). \tag{65}$$

Combining (54)–(65), an approximated lower bound on the downlink spectral efficiency for the kth device can be obtained as

$$\underline{R}_k^d \approx \log_2\left(1 + \frac{\frac{P_k^d \mathrm{e}^{-\sigma_\nu^2}}{\mathrm{tr}(\boldsymbol{R}_k\boldsymbol{R}_k^{\mathrm{sub}})}|\mathrm{tr}(\boldsymbol{R}_k\boldsymbol{R}_k^{\mathrm{sub}})|^2}{\sum_{i=1,i\neq k}^{K}\frac{P_i^d}{\mathrm{tr}(\boldsymbol{R}_k\boldsymbol{R}_k^{\mathrm{sub}})}\mathrm{tr}(\boldsymbol{R}_i\boldsymbol{R}_i^{\mathrm{sub}}\boldsymbol{R}_k^{e}\boldsymbol{R}_i^{\mathrm{sub}}) + \sigma_d^2}\right). \tag{66}$$

According to (66), we found that the downlink spectral efficiency is also a decreasing function with respect to σ_μ and σ_ν, which is similar to the uplink case.

4 Numerical results

In this section, we conduct extensive simulations to reveal the impacts of system parameters on the performance of IRS-assisted THz multiuser massive MIMO system. Without extra specification, simulation parameters are set as follows: $f = 0.3$ THz, $k(f) = 0.5$, $c(f) = 0.1$, $\lambda = 10^{-3}$ m, $d = \lambda/2$, $N_t = 64$, $N_s = 16$, $M = 4$, $N_r = 64$, $K = 48$, $L = 2$, $L_k = 2$, $\sigma_\alpha^2 = \sigma_{\beta,k}^2 = 1$, $\eta = 1$, $\rho_i = 1$, $\forall i \in [1, K]$. For convenience, we use $\mathrm{SNR}^u = 10\log_{10} P^u/\sigma_u^2$ and $\mathrm{SNR}^d = 10\log_{10} P^d/\sigma_d^2$ to denote the uplink and the downlink transmit SNR (in dB). Since we consider the spectral efficiency, the unit bandwidth is adopted in the paper.

First of all, we verify the accuracy of the derived theoretical expressions for the spectral efficiency over uplink and downlink. Since the transmit power of the BS tends to be much larger than that of the devices, we set the downlink data transmit power to ten times the uplink one. As can be seen in Figure 2, the theoretical values of the uplink match the simulation values better than those of the downlink. Generally speaking, the gaps between the theoretical expressions and the simulation results can be negligible in the whole SNR region for both uplink and downlink. Thus, the approximations of the spectral efficiency can be used to evaluate the performance of the IRS-assisted THz multiuser massive MIMO system accurately.

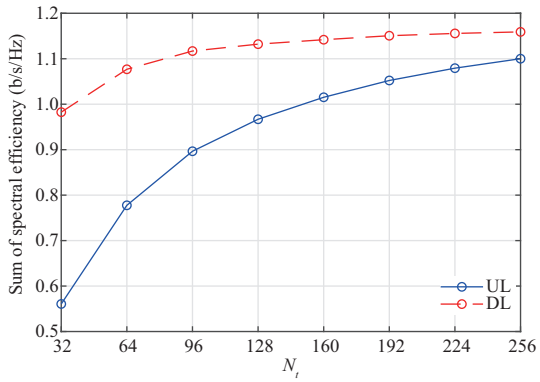

Figure 3 (Color online) The effect of the number of BS antennas on spectral efficiency.

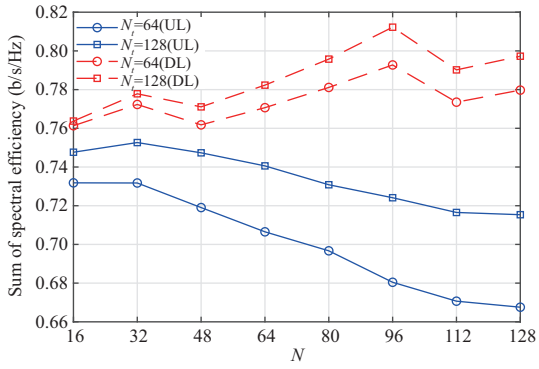

Figure 4 (Color online) The effect of the number of reflecting units on spectral efficiency.

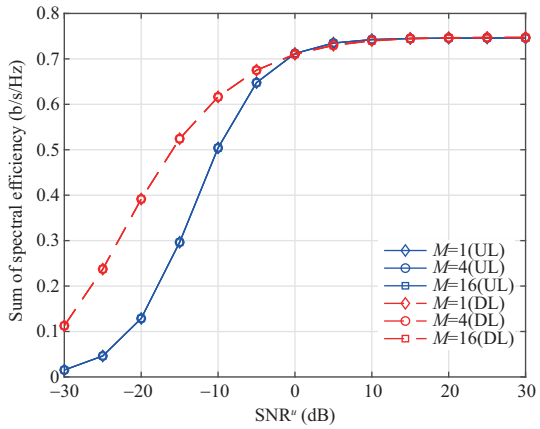

Figure 5 (Color online) The impact of different sub-connected architectures on spectral efficiency.

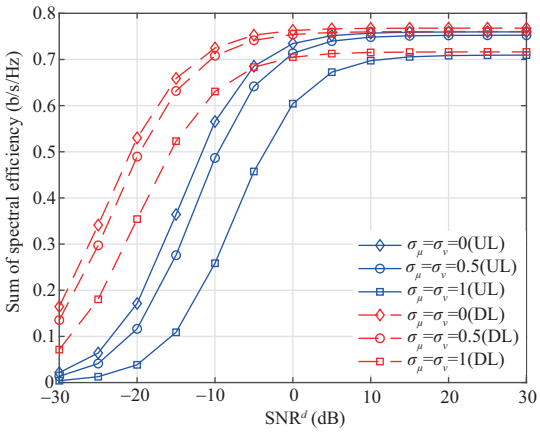

Figure 6 (Color online) The impact of the analog precoding error on spectral efficiency.

Moreover, it is found that the spectral efficiency improves sharply in the low SNR region and will be saturated in the high SNR region.

Next, we investigate the effect of the number of BS antennas. As Figure 3 shows, the sum of spectral efficiency first improves as the number of BS antennas increases in both uplink and downlink but will be saturated in the large N_t region. Thus, we should strike a balance between the performance gain and the antenna cost for practical IRS-assisted THz multiuser massive MIMO systems.

Then, we explore the effect of the number of reflecting units on spectral efficiency. As can be seen in Figure 4, the spectral efficiency is not a monotonic function as the number of reflecting units increases. This is because the IRS in the multiuser scenarios not only enhances the desired signal, but also increases inter-device interference. Thus, we should select a proper number of reflecting units in order to improve the overall performance.

Moreover, we investigate the impact of different sub-connected architectures on spectral efficiency. Interestingly, it is found in Figure 5 that the different architectures with different M do not change the spectral efficiency. In this case, we can choose a large M to reduce the number of RF chains, and thus cut down the costs for IRS-assisted THz multiuser massive MIMO system.

Finally, we study the impact of the analog precoding error on spectral efficiency. As shown in Figure 6, the analog precoding error has a significant impact on spectral efficiency. The smaller the analog precoding error, the higher the spectral efficiency. When the σ_μ and the σ_{nu} tend to zero, the analog precoding can operate perfectly and there is no precoding error. Thus, eliminating the analog precoding error is critical to improving the performance for IRS-assisted THz multiuser massive MIMO.

5 Conclusion

In this paper, we proposed a framework with sub-connected architecture for IRS-assisted THz multiuser massive MIMO systems, including uplink and downlink data transmission. Moreover, we investigated the impact of the analog precoding with phase-shifting error on the spectral efficiency. We found that the spectral efficiency is a decreasing function with respect to the analog precoding error over the uplink and downlink. Thus, eliminating the analog precoding error can significantly improve the system performance. In addition, we found that the spectral efficiency is not a monotonic function with respect to the number of reflecting units because the IRS does not only enhance the signal quality but also inter-device interference. Hence, we need to choose a proper number of reflecting units.

Acknowledgements This work was supported by National Key R&D Program of China (Grant No. 2020YFB1805703), National Natural Science Foundation of China (Grant No. 61871344), and Zhejiang Provincial Natural Science Foundation of China (Grant No. LR20F010002).

References

1 Chen X M, Ng D W K, Yu W, et al. Massive access for 5G and beyond. IEEE J Sel Areas Commun, 2021, 39: 615–637
2 Ahmed N, De D, Hussain I. Internet of Things (IoT) for smart precision agriculture and farming in rural areas. IEEE Int Things J, 2018, 5: 4890–4899
3 Qi Q, Chen X M, Zhong C J, et al. Physical layer security for massive access in cellular Internet of Things. Sci China Inf Sci, 2020, 63: 121301
4 Han C, Wu Y Z, Chen Z, et al. Terahertz communications (TeraCom): challenges and impact on 6G wireless systems. 2019. ArXiv:1912.06040v2
5 Zhang Z Q, Xiao Y, Ma Z, et al. 6G wireless networks: vision, requirements, architecture, and key technologies. IEEE Veh Technol Mag, 2019, 14: 28–41
6 Boulogeorgos A A A, Alexiou A, Merkle T, et al. Terahertz technologies to deliver optical network quality of experience in wireless systems beyond 5G. IEEE Commun Mag, 2018, 56: 144–151
7 Hu X L, Zhong C J, Chen X M, et al. Cell-free massive MIMO systems with low resolution ADCs. IEEE Trans Commun, 2019, 67: 6844–6857
8 Zhao F R, Zhong C J, Chen X M, et al. Energy efficiency of massive MIMO downlink WPT with mixed-ADCs. IEEE Commun Lett, 2019, 23: 2316–2320
9 Jia R D, Chen X M, Zhong C J, et al. Design of non-orthogonal beamspace multiple access for cellular Internet-of-Things. IEEE J Sel Top Signal Process, 2019, 13: 538–552
10 Chen X M, Zhang Z Y, Zhong C J, et al. Exploiting multiple-antenna techniques for non-orthogonal multiple access. IEEE J Sel Areas Commun, 2017, 35: 2207–2220
11 Rappaport T S, Xing Y C, Kanhere O, et al. Wireless communications and applications above 100 GHz: opportunities and challenges for 6G and beyond. IEEE Access, 2019, 7: 78729–78757
12 Wang P, Li Y H, Song L Y, et al. Multi-gigabit millimeter wave wireless communications for 5G: from fixed access to cellular networks. IEEE Commun Mag, 2015, 53: 168–178
13 Yang P, Xiao Y, Xiao M, et al. 6G wireless communications: vision and potential techniques. IEEE Netw, 2019, 33: 70–75
14 Yuan Y F, Zhao Y J, Zong B Q, et al. Potential key technologies for 6G mobile communications. Sci China Inf Sci, 2020, 63: 183301
15 Song H J, Nagatsuma T. Present and future of Terahertz communications. IEEE Trans Terahertz Sci Technol, 2011, 1: 256–263
16 Jornet J M, Akyildiz I F. Channel modeling and capacity analysis for electromagnetic wireless nanonetworks in the Terahertz band. IEEE Trans Wirel Commun, 2011, 10: 3211–3221
17 Han C, Bicen A O, Akyildiz I F. Multi-ray channel modeling and wideband characterization for wireless communications in the Terahertz band. IEEE Trans Wirel Commun, 2015, 14: 2402–2412
18 Afsharinejad A, Davy A, Jennings B, et al. A path-loss model incorporating shadowing for THz band propagation in vegetation. In: Proceedings of IEEE Global Communications Conference (GLOBECOM), 2015. 1–6
19 Ekti A R, Boyaci A, Alparslan A, et al. Statistical modeling of propagation channels for Terahertz band. In: Proceedings of IEEE Conference on Standards for Communications and Networking (CSCN), 2017. 275–280
20 You X H, Wang C X, Huang J, et al. Towards 6G wireless communication networks: vision, enabling technologies, and new paradigm shifts. Sci China Inf Sci, 2021, 64: 110301
21 Hu X L, Wang J W, Zhong C J. Statistical CSI based design for intelligent reflecting surface assisted MISO systems. Sci China Inf Sci, 2020, 63: 222303
22 Yu G H, Chen X M, Zhong C J, et al. Design, analysis, and optimization of a large intelligent reflecting surface-aided B5G cellular Internet of Things. IEEE Int Things J, 2020, 7: 8902–8916
23 Hu S, Rusek F, Edfors O. The potential of using large antenna arrays on intelligent surfaces. In: Proceedings of the 85th Vehicular Technology Conference (VTC Spring), 2017. 1–6
24 Tang W K, Li X, Dai J Y, et al. Wireless communications with programmable metasurface: transceiver design and experimental results. China Commun, 2019, 16: 46–61
25 Ning B Y, Chen Z, Chen W R, et al. Channel estimation and transmission for intelligent reflecting surface assisted THz communications. In: Proceedigs of IEEE International Conference on Communications (ICC), 2020. 1–7
26 Li Z X, Chen Z, Ma X Y, et al. Channel estimation for intelligent reflecting surface enabled Terahertz MIMO systems: a deep learning perspective. In: Proceedigs of IEEE/CIC International Conference on Communications in China (ICCC Workshops), 2020. 75–79
27 Ma X Y, Chen Z, Chen W J, et al. Joint channel estimation and data rate maximization for intelligent reflecting surface assisted Terahertz MIMO communication systems. IEEE Access, 2020, 8: 99565–99581
28 Chen W J, Ma X Y, Li Z X, et al. Sum-rate maximization for intelligent reflecting surface based Terahertz communication systems. In: Proceedigs of IEEE/CIC International Conference on Communications Workshops in China (ICCC Workshops),

2019. 153–157
29 Qiao J P, Alouini M S. Secure transmission for intelligent reflecting surface-assisted mmwave and Terahertz systems. IEEE Wirel Commun Lett, 2020, 9: 1743–1747
30 Hu X L, Zhong C J, Chen X M, et al. Cluster grouping and power control for angle-domain MmWave MIMO NOMA systems. IEEE J Sel Top Signal Process, 2019, 13: 1167–1180
31 Alkhateeb A, El Ayach O, Leus G, et al. Channel estimation and hybrid precoding for millimeter wave cellular systems. IEEE J Sel Top Signal Process, 2014, 8: 831–846
32 Han S F, Chih-Lin I, Xu Z K, et al. Large-scale antenna systems with hybrid analog and digital beamforming for millimeter wave 5G. IEEE Commun Mag, 2015, 53: 186–194
33 Maruthi S P, Panigrahi T, Hassan M. Improving the reliability of pulse-based Terahertz communication using intelligent reflective surface. In: Proceedigs of IEEE International Conference on Communications Workshops (ICC Workshops), 2020. 1–6
34 Croswell W. Antenna theory, analysis, and design. IEEE Antennas Propag Soc Newsl, 1982, 24: 28–29
35 Hur S, Kim T, Love D J, et al. Millimeter wave beamforming for wireless backhaul and access in small cell networks. IEEE Trans Commun, 2013, 61: 4391–4403
36 Chen X M, Zhang Z Y, Zhong C J, et al. Fully non-orthogonal communication for massive access. IEEE Trans Commun, 2018, 66: 1717–1731
37 Björnson E, Hoydis J, Sanguinetti L. Massive MIMO networks: spectral, energy, and hardware efficiency. FNT Signal Process, 2017, 11: 154–655
38 Chen J, Chen X M, Gerstacker W H, et al. Resource allocation for a massive MIMO relay aided secure communication. IEEE Trans Inform Forensic Secur, 2016, 11: 1700–1711

Appendix A Lemmas 1–3

Lemma 1. Consider the vector $\boldsymbol{x}$, which can be expressed as

$$\boldsymbol{x} = \boldsymbol{A}_x \boldsymbol{v} \tag{A1}$$

with $\boldsymbol{A}_x \in \mathcal{C}^{M\times N}$ and $\boldsymbol{v} \sim \mathcal{N}_c(\boldsymbol{0}, \sigma_x^2 \boldsymbol{I}_N)$. It holds true that

$$\mathrm{E}[\boldsymbol{x}\boldsymbol{x}^{\mathrm{H}}] = \sigma_x^2 \boldsymbol{A}_x \boldsymbol{A}_x^{\mathrm{H}}, \tag{A2}$$

and

$$\mathrm{E}[\boldsymbol{x}^{\mathrm{H}}\boldsymbol{B}\boldsymbol{x}] = \sigma_x^2 \mathrm{tr}(\boldsymbol{B}\boldsymbol{A}_x \boldsymbol{A}_x^{\mathrm{H}}) \tag{A3}$$

with $\boldsymbol{B} \in \mathcal{C}^{M\times M}$.

Proof. Please refer to Appendix B.

Lemma 2. Consider the matrix $\boldsymbol{Y}$, which can be expressed as

$$\boldsymbol{Y} = \boldsymbol{A}_1 \boldsymbol{U} \boldsymbol{A}_2, \tag{A4}$$

where $\boldsymbol{A}_1 \in \mathcal{C}^{M\times L}$, $\boldsymbol{A}_2 \in \mathcal{C}^{L\times N}$, and $\boldsymbol{U} = \mathrm{diag}(\alpha_1, \ldots, \alpha_L)$, $\alpha_i \sim \mathcal{N}_c(0, \sigma_y^2)$. It holds true that

$$\mathrm{E}[\boldsymbol{Y}\boldsymbol{B}_1\boldsymbol{Y}^{\mathrm{H}}] = \sigma_y^2 \boldsymbol{A}_1 \mathrm{diag}(\boldsymbol{A}_2\boldsymbol{B}_1\boldsymbol{A}_2^{\mathrm{H}})\boldsymbol{A}_1^{\mathrm{H}}, \tag{A5}$$

and

$$\mathrm{E}[\boldsymbol{Y}^{\mathrm{H}}\boldsymbol{B}_2\boldsymbol{Y}] = \sigma_y^2 \boldsymbol{A}_2^{\mathrm{H}} \mathrm{diag}(\boldsymbol{A}_1^{\mathrm{H}}\boldsymbol{B}_2\boldsymbol{A}_1)\boldsymbol{A}_2 \tag{A6}$$

with $\boldsymbol{B}_1 \in \mathcal{C}^{N\times N}$ and $\boldsymbol{B}_2 \in \mathcal{C}^{M\times M}$.

Proof. Please refer to Appendix B.

Lemma 3. Consider the N-dimensional random vector $\boldsymbol{h}$ with $\mathrm{E}[\boldsymbol{h}\boldsymbol{h}^{\mathrm{H}}] = \boldsymbol{R}$ and $\boldsymbol{R} \in \mathcal{C}^{N\times N}$. It holds true that

$$\mathrm{E}[\boldsymbol{h}^{\mathrm{H}}\boldsymbol{B}\boldsymbol{h}] = \mathrm{tr}(\boldsymbol{B}\boldsymbol{R}) \tag{A7}$$

with $\boldsymbol{B} \in \mathcal{C}^{N\times N}$.

Proof. Please refer to Appendix B.

Appendix B The proof of Lemmas 1–3

Appendix B.1 The proof of Lemma 1

For the term $\mathrm{E}[\boldsymbol{x}\boldsymbol{x}^{\mathrm{H}}]$, we have

$$\mathrm{E}[\boldsymbol{x}\boldsymbol{x}^{\mathrm{H}}] = \mathrm{E}[\boldsymbol{A}_x\boldsymbol{v}\boldsymbol{v}^{\mathrm{H}}\boldsymbol{A}_x^{\mathrm{H}}] = \boldsymbol{A}_x \mathrm{E}[\boldsymbol{v}\boldsymbol{v}^{\mathrm{H}}]\boldsymbol{A}_x^{\mathrm{H}} = \sigma_x^2 \boldsymbol{A}_x \boldsymbol{A}_x^{\mathrm{H}}. \tag{B1}$$

As for the term $\mathrm{E}[\boldsymbol{x}^{\mathrm{H}}\boldsymbol{B}\boldsymbol{x}]$, we have

$$\mathrm{E}[\boldsymbol{x}^{\mathrm{H}}\boldsymbol{B}\boldsymbol{x}] = \mathrm{E}[\boldsymbol{v}^{\mathrm{H}}\boldsymbol{A}_x^{\mathrm{H}}\boldsymbol{B}\boldsymbol{A}_x\boldsymbol{v}]. \tag{B2}$$

Without loss of generality, we assume that

$$\boldsymbol{v} = [v_1, \ldots, v_n, \ldots, v_N], \tag{B3}$$

$$\boldsymbol{A}_x^{\mathrm{H}}\boldsymbol{B}\boldsymbol{A}_x = \begin{bmatrix} w_{1,1} & \cdots & w_{1,n} & \cdots & w_{1,N} \\ \vdots & & \vdots & & \vdots \\ w_{n,1} & \cdots & w_{n,n} & \cdots & w_{n,N} \\ \vdots & & \vdots & & \vdots \\ w_{N,1} & \cdots & w_{N,n} & \cdots & w_{N,N} \end{bmatrix}, \tag{B4}$$

Then, we can obtain

$$\mathrm{E}[\boldsymbol{v}^{\mathrm{H}}\boldsymbol{A}_x^{\mathrm{H}}\boldsymbol{B}\boldsymbol{A}_x\boldsymbol{v}] = \mathrm{E}[w'_{1,1}v_1 + \cdots + w'_{1,n}v_n + \cdots + w'_{1,N}v_N] \tag{B5}$$

with

$$w'_{1,n} = v_1^{\mathrm{H}}w_{1,n} + \cdots + v_n^{\mathrm{H}}w_{n,n} + \cdots + v_N^{\mathrm{H}}w_{N,n}. \tag{B6}$$

It holds true that $\mathrm{E}[v_i^{\mathrm{H}}wv_j] = 0, \forall i \neq j$ because the elements in $\boldsymbol{v}$ are independent of each other. Thus, we have

$$\mathrm{E}[\boldsymbol{x}^{\mathrm{H}}\boldsymbol{B}\boldsymbol{x}] = \mathrm{E}[\boldsymbol{v}^{\mathrm{H}}\boldsymbol{A}_x^{\mathrm{H}}\boldsymbol{B}\boldsymbol{A}_x\boldsymbol{v}] = \sigma_x^2(w_{1,1} + \cdots + w_{n,n} + \cdots + w_{N,N}) = \sigma_x^2\mathrm{tr}(\boldsymbol{A}_x^{\mathrm{H}}\boldsymbol{B}\boldsymbol{A}_x). \tag{B7}$$

The proof of Lemma 1 finished.

Appendix B.2 The proof of Lemma 2

For the first term $\mathrm{E}[\boldsymbol{Y}\boldsymbol{B}_1\boldsymbol{Y}^{\mathrm{H}}]$, we have

$$\mathrm{E}[\boldsymbol{Y}\boldsymbol{B}_1\boldsymbol{Y}^{\mathrm{H}}] = \mathrm{E}[\boldsymbol{A}_1\boldsymbol{U}\boldsymbol{A}_2\boldsymbol{B}_1\boldsymbol{A}_2^{\mathrm{H}}\boldsymbol{U}^{\mathrm{H}}\boldsymbol{A}_1^{\mathrm{H}}]. \tag{B8}$$

Without loss of generality, we assume that

$$\boldsymbol{A}_2\boldsymbol{B}_1\boldsymbol{A}_2^{\mathrm{H}} = \begin{bmatrix} p_{1,1} & \cdots & p_{1,n} & \cdots & p_{1,L} \\ \vdots & & \vdots & & \vdots \\ p_{n,1} & \cdots & p_{n,n} & \cdots & p_{n,L} \\ \vdots & & \vdots & & \vdots \\ p_{L,1} & \cdots & p_{L,n} & \cdots & p_{L,L} \end{bmatrix}. \tag{B9}$$

Then, $\boldsymbol{U}\boldsymbol{A}_2\boldsymbol{B}_1\boldsymbol{A}_2^{\mathrm{H}}\boldsymbol{U}^{\mathrm{H}}$ can be computed as

$$\boldsymbol{U}\boldsymbol{A}_2\boldsymbol{B}_1\boldsymbol{A}_2^{\mathrm{H}}\boldsymbol{U}^{\mathrm{H}} = \begin{bmatrix} \alpha_1 p_{1,1}\alpha_1^{\mathrm{H}} & \cdots & \alpha_1 p_{1,n}\alpha_n^{\mathrm{H}} & \cdots & \alpha_1 p_{1,L}\alpha_L^{\mathrm{H}} \\ \vdots & & \vdots & & \vdots \\ \alpha_n p_{n,1}\alpha_1^{\mathrm{H}} & \cdots & \alpha_n p_{n,n}\alpha_n^{\mathrm{H}} & \cdots & \alpha_n p_{n,L}\alpha_L^{\mathrm{H}} \\ \vdots & & \vdots & & \vdots \\ \alpha_L p_{L,1}\alpha_1^{\mathrm{H}} & \cdots & \alpha_L p_{L,n}\alpha_n^{\mathrm{H}} & \cdots & \alpha_L p_{L,L}\alpha_L^{\mathrm{H}} \end{bmatrix}. \tag{B10}$$

$\mathrm{E}[p\alpha_i\alpha_j] = 0$ $(\forall i \neq j)$ holds true due to the fact that the elements $\alpha_1, \ldots, \alpha_L$ are independent of each other. Thus, we have

$$\begin{aligned} \mathrm{E}[\boldsymbol{Y}\boldsymbol{B}_1\boldsymbol{Y}^{\mathrm{H}}] &= \boldsymbol{A}_1\mathrm{E}[\boldsymbol{U}\boldsymbol{A}_2\boldsymbol{B}_1\boldsymbol{A}_2^{\mathrm{H}}\boldsymbol{U}^{\mathrm{H}}]\boldsymbol{A}_1^{\mathrm{H}} & \text{(B11)} \\ &= \sigma_y^2\boldsymbol{A}_1 \begin{bmatrix} p_{1,1} & 0 & \cdots & \cdots & 0 \\ 0 & \ddots & & & \vdots \\ \vdots & & p_{n,n} & & \vdots \\ \vdots & & & \ddots & 0 \\ 0 & \cdots & \cdots & 0 & p_{L,L} \end{bmatrix} \boldsymbol{A}_1^{\mathrm{H}} \\ &= \sigma_y^2\boldsymbol{A}_1\mathrm{diag}[\boldsymbol{A}_2\boldsymbol{B}_1\boldsymbol{A}_2^{\mathrm{H}}]\boldsymbol{A}_1^{\mathrm{H}}. & \text{(B12)} \end{aligned}$$

Similarly, we can obtain

$$\mathrm{E}[\boldsymbol{Y}^{\mathrm{H}}\boldsymbol{B}_2\boldsymbol{Y}] = \sigma_y^2\boldsymbol{A}_2^{\mathrm{H}}\mathrm{diag}(\boldsymbol{A}_1^{\mathrm{H}}\boldsymbol{B}_2\boldsymbol{A}_1)\boldsymbol{A}_2. \tag{B13}$$

The proof of Lemma 2 finished.

Appendix B.3 The proof of Lemma 3

Without loss of generality, we assume that

$$\boldsymbol{h} = [h_1, \ldots, h_n, \ldots, h_N], \tag{B14}$$

$$\boldsymbol{R} = \mathrm{E}[\boldsymbol{h}\boldsymbol{h}^{\mathrm{H}}] = \begin{bmatrix} r_{1,1} & \cdots & r_{1,n} & \cdots & r_{1,N} \\ \vdots & & \vdots & & \vdots \\ r_{n,1} & \cdots & r_{n,n} & \cdots & r_{n,N} \\ \vdots & & \vdots & & \vdots \\ r_{N,1} & \cdots & r_{N,n} & \cdots & r_{N,N} \end{bmatrix}, \tag{B15}$$

and

$$\boldsymbol{B}=\begin{bmatrix} b_{1,1} & \cdots & b_{1,n} & \cdots & b_{1,N} \\ \vdots & & \vdots & & \vdots \\ b_{n,1} & \cdots & b_{n,n} & \cdots & b_{n,N} \\ \vdots & & \vdots & & \vdots \\ b_{N,1} & \cdots & b_{N,n} & \cdots & b_{N,N} \end{bmatrix}. \tag{B16}$$

Thus, the term $\mathrm{E}[\boldsymbol{h}^{\mathrm{H}}\boldsymbol{B}\boldsymbol{h}]$ can be computed as

$$\begin{aligned}\mathrm{E}[\boldsymbol{h}^{\mathrm{H}}\boldsymbol{B}\boldsymbol{h}] &= \mathrm{E}[(h_1^{\mathrm{H}}b_{1,1}+\cdots+h_N^{\mathrm{H}}b_{N,1})h_1+\cdots+(h_1^{\mathrm{H}}b_{1,N}+\cdots+h_N^{H}b_{N,N})h_N] \\ &= \sum_{i=1}^{N}\sum_{j=1}^{N} r_{i,j}b_{i,j}. \end{aligned}\tag{B17}$$

Then, the term $\mathrm{tr}(\boldsymbol{B}\boldsymbol{R})$ can be expressed as

$$\begin{aligned}\mathrm{tr}(\boldsymbol{B}\boldsymbol{R}) &= (b_{1,1}r_{1,1}+\cdots+b_{1,N}r_{N,1})+\cdots+(b_{N,1}r_{1,N}+\cdots+b_{N,N}r_{N,N}) \\ &= \sum_{i=1}^{N}\sum_{j=1}^{N} r_{i,j}b_{i,j}. \end{aligned}\tag{B18}$$

Hence, we can obtain

$$\mathrm{E}[\boldsymbol{h}^{\mathrm{H}}\boldsymbol{B}\boldsymbol{h}]=\mathrm{tr}(\boldsymbol{B}\boldsymbol{R}) \tag{B19}$$

for arbitrarily distributed random vector $\boldsymbol{h}$. The proof of Lemma 3 finished.

Appendix C The computation of autocorrelation matrix R_i^e

First of all, we begin with calculating the autocorrelation matrix of $\boldsymbol{h}_k$:

$$\begin{aligned}\boldsymbol{R}_k &= \mathrm{E}[\boldsymbol{h}_k\boldsymbol{h}_k^{\mathrm{H}}] \\ &= \mathrm{E}[\boldsymbol{H}\boldsymbol{\Theta}\boldsymbol{h}_{r,k}(\boldsymbol{H}\boldsymbol{\Theta}\boldsymbol{h}_{r,k})^{\mathrm{H}}] \\ &= \mathrm{E}[\boldsymbol{H}(\bar{\boldsymbol{\Theta}}+\tilde{\boldsymbol{\Theta}})(\bar{\boldsymbol{h}}_{r,k}+\tilde{\boldsymbol{h}}_{r,k})(\bar{\boldsymbol{h}}_{r,k}+\tilde{\boldsymbol{h}}_{r,k})^{\mathrm{H}}(\bar{\boldsymbol{\Theta}}^{\mathrm{H}}+\tilde{\boldsymbol{\Theta}}^{\mathrm{H}})\boldsymbol{H}^{\mathrm{H}}] \\ &= \mathrm{E}[\boldsymbol{H}(\bar{\boldsymbol{\Theta}}\bar{\boldsymbol{h}}_{r,k}\bar{\boldsymbol{h}}_{r,k}^{\mathrm{H}}\bar{\boldsymbol{\Theta}}^{\mathrm{H}}+\bar{\boldsymbol{\Theta}}\tilde{\boldsymbol{h}}_{r,k}\tilde{\boldsymbol{h}}_{r,k}^{\mathrm{H}}\bar{\boldsymbol{\Theta}}^{\mathrm{H}})\boldsymbol{H}^{\mathrm{H}}]+\mathrm{E}[\boldsymbol{H}(\bar{\boldsymbol{\Theta}}\bar{\boldsymbol{h}}_{r,k}\tilde{\boldsymbol{h}}_{r,k}^{\mathrm{H}}\tilde{\boldsymbol{\Theta}}^{\mathrm{H}}+\bar{\boldsymbol{\Theta}}\tilde{\boldsymbol{h}}_{r,k}\bar{\boldsymbol{h}}_{r,k}^{\mathrm{H}}\tilde{\boldsymbol{\Theta}}^{\mathrm{H}})\boldsymbol{H}^{\mathrm{H}}] \\ &\quad+\mathrm{E}[\boldsymbol{H}(\tilde{\boldsymbol{\Theta}}\bar{\boldsymbol{h}}_{r,k}\tilde{\boldsymbol{h}}_{r,k}^{\mathrm{H}}\bar{\boldsymbol{\Theta}}^{\mathrm{H}}+\tilde{\boldsymbol{\Theta}}\bar{\boldsymbol{h}}_{r,k}\bar{\boldsymbol{h}}_{r,k}^{\mathrm{H}}\bar{\boldsymbol{\Theta}}^{\mathrm{H}})\boldsymbol{H}^{\mathrm{H}}]+\mathrm{E}[\boldsymbol{H}(\tilde{\boldsymbol{\Theta}}\bar{\boldsymbol{h}}_{r,k}\bar{\boldsymbol{h}}_{r,k}^{\mathrm{H}}\tilde{\boldsymbol{\Theta}}^{\mathrm{H}}+\tilde{\boldsymbol{\Theta}}\tilde{\boldsymbol{h}}_{r,k}\tilde{\boldsymbol{h}}_{r,k}^{\mathrm{H}}\tilde{\boldsymbol{\Theta}}^{\mathrm{H}})\boldsymbol{H}^{\mathrm{H}}] \qquad \text{(C1)} \\ &= \mathrm{E}[\boldsymbol{H}\bar{\boldsymbol{\Theta}}\boldsymbol{R}_{r,k}\bar{\boldsymbol{\Theta}}^{\mathrm{H}}\boldsymbol{H}^{\mathrm{H}}]+2\mathrm{Re}(\mathrm{E}[\boldsymbol{H}\bar{\boldsymbol{\Theta}}\bar{\boldsymbol{h}}_{r,k}\tilde{\boldsymbol{h}}_{r,k}^{\mathrm{H}}\tilde{\boldsymbol{\Theta}}^{\mathrm{H}}\boldsymbol{H}^{\mathrm{H}}] \\ &\quad+\mathrm{E}[\boldsymbol{H}\bar{\boldsymbol{\Theta}}\tilde{\boldsymbol{h}}_{r,k}\bar{\boldsymbol{h}}_{r,k}^{\mathrm{H}}\tilde{\boldsymbol{\Theta}}^{\mathrm{H}}\boldsymbol{H}^{\mathrm{H}}])+\mathrm{E}[\boldsymbol{H}\tilde{\boldsymbol{\Theta}}\boldsymbol{R}_{r,k}\tilde{\boldsymbol{\Theta}}^{\mathrm{H}}\boldsymbol{H}^{\mathrm{H}}]. \qquad \text{(C2)}\end{aligned}$$

Eq. (C1) holds true because that $\boldsymbol{H}$ is independent of $\boldsymbol{\Theta}$ and $\boldsymbol{h}_{r,k}$ and $\mathrm{E}[\tilde{\boldsymbol{\Theta}}]=\mathrm{E}[\tilde{\boldsymbol{h}_{r,k}}]=0$. According to Lemmas 1–3 and by applying the property of channel hardening for massive MIMO systems, we can obtain (C2) from (C1). Next, we can compute the first term of (C2) as follows:

$$\begin{aligned}\mathrm{E}[\boldsymbol{H}\bar{\boldsymbol{\Theta}}\boldsymbol{R}_{r,k}\bar{\boldsymbol{\Theta}}^{\mathrm{H}}\boldsymbol{H}^{\mathrm{H}}] &= \mathrm{E}[\bar{\boldsymbol{H}}\bar{\boldsymbol{\Theta}}\boldsymbol{R}_{r,k}\bar{\boldsymbol{\Theta}}^{\mathrm{H}}\bar{\boldsymbol{H}}^{\mathrm{H}}]+\mathrm{E}[\tilde{\boldsymbol{H}}\bar{\boldsymbol{\Theta}}\boldsymbol{R}_{r,k}\bar{\boldsymbol{\Theta}}^{\mathrm{H}}\tilde{\boldsymbol{H}}^{\mathrm{H}}] \qquad \text{(C3)} \\ &= \bar{\boldsymbol{H}}\bar{\boldsymbol{\Theta}}\boldsymbol{R}_{r,k}\bar{\boldsymbol{\Theta}}^{\mathrm{H}}\bar{\boldsymbol{H}}^{\mathrm{H}}+\sigma_\alpha^2\boldsymbol{A}_r\mathrm{diag}(\boldsymbol{A}_t^{\mathrm{H}}\bar{\boldsymbol{\Theta}}\boldsymbol{R}_{r,k}\bar{\boldsymbol{\Theta}}^{\mathrm{H}}\boldsymbol{A}_t)\boldsymbol{A}_r^{\mathrm{H}}. \qquad \text{(C4)}\end{aligned}$$

Eq. (C3) holds true due to that $\mathrm{E}[\tilde{\boldsymbol{H}}]=0$ and Eq. (C4) holds true based on Lemma 2. Similarly, the second term of (C2) can be computed as follows:

$$\begin{aligned}&2\mathrm{Re}(\mathrm{E}[\boldsymbol{H}\bar{\boldsymbol{\Theta}}\bar{\boldsymbol{h}}_{r,k}\tilde{\boldsymbol{h}}_{r,k}^{\mathrm{H}}\tilde{\boldsymbol{\Theta}}^{\mathrm{H}}\boldsymbol{H}^{\mathrm{H}}]+\mathrm{E}[\boldsymbol{H}\bar{\boldsymbol{\Theta}}\tilde{\boldsymbol{h}}_{r,k}\bar{\boldsymbol{h}}_{r,k}^{\mathrm{H}}\tilde{\boldsymbol{\Theta}}^{\mathrm{H}}\boldsymbol{H}^{\mathrm{H}}]) \\ &=2\mathrm{Re}\Bigg\{\frac{\eta\sqrt{\rho_k}}{\sqrt{\sum_{i=1}^{K}\rho_i\mathrm{E}[\|\boldsymbol{h}_{r,i}\|^2]}}(\mathrm{E}[\boldsymbol{H}\bar{\boldsymbol{\Theta}}\bar{\boldsymbol{h}}_{r,k}\mathrm{vec}(\mathrm{diag}(\boldsymbol{R}_{r,k}-\bar{\boldsymbol{h}}_{r,k}\bar{\boldsymbol{h}}_{r,k}^{\mathrm{H}}))^{\mathrm{T}}\boldsymbol{H}^{\mathrm{H}}] \\ &\quad+\mathrm{E}[\boldsymbol{H}\bar{\boldsymbol{\Theta}}(\boldsymbol{R}_{r,k}-\bar{\boldsymbol{h}}_{r,k}\bar{\boldsymbol{h}}_{r,k}^{\mathrm{H}})\mathrm{diag}(\bar{\boldsymbol{h}}_{r,k}^{\mathrm{H}})\boldsymbol{H}^{\mathrm{H}}])\Bigg\} \\ &=2\mathrm{Re}\Bigg\{\frac{\eta\sqrt{\rho_k}}{\sqrt{\sum_{i=1}^{K}\rho_i\mathrm{tr}(\boldsymbol{R}_{r,i})}}(\bar{\boldsymbol{H}}\bar{\boldsymbol{\Theta}}\bar{\boldsymbol{h}}_{r,k}\mathrm{vec}(\mathrm{diag}(\boldsymbol{R}_{r,k}-\bar{\boldsymbol{h}}_{r,k}\bar{\boldsymbol{h}}_{r,k}^{\mathrm{H}}))^{\mathrm{T}}\bar{\boldsymbol{H}}^{\mathrm{H}} \\ &\quad+\sigma_\alpha^2\boldsymbol{A}_r\mathrm{diag}(\boldsymbol{A}_t^{\mathrm{H}}\bar{\boldsymbol{\Theta}}\bar{\boldsymbol{h}}_{r,k}\mathrm{vec}(\mathrm{diag}(\boldsymbol{R}_{r,k}-\bar{\boldsymbol{h}}_{r,k}\bar{\boldsymbol{h}}_{r,k}^{\mathrm{H}}))^{\mathrm{T}}\boldsymbol{A}_t)\boldsymbol{A}_r^{\mathrm{H}} \\ &\quad+\bar{\boldsymbol{H}}\bar{\boldsymbol{\Theta}}(\boldsymbol{R}_{r,k}-\bar{\boldsymbol{h}}_{r,k}\bar{\boldsymbol{h}}_{r,k}^{\mathrm{H}})\mathrm{diag}(\bar{\boldsymbol{h}}_{r,k}^{\mathrm{H}})\bar{\boldsymbol{H}}^{\mathrm{H}} \\ &\quad+\sigma_\alpha^2\boldsymbol{A}_r\mathrm{diag}(\boldsymbol{A}_t^{\mathrm{H}}\bar{\boldsymbol{\Theta}}(\boldsymbol{R}_{r,k}-\bar{\boldsymbol{h}}_{r,k}\bar{\boldsymbol{h}}_{r,k}^{\mathrm{H}})\mathrm{diag}(\bar{\boldsymbol{h}}_{r,k}^{\mathrm{H}})\boldsymbol{A}_t)\boldsymbol{A}_r^{\mathrm{H}})\Bigg\}. \qquad \text{(C5)}\end{aligned}$$

Then, we compute the third term of (C2) as follows:

$$\mathrm{E}[\boldsymbol{H}\tilde{\boldsymbol{\Theta}}\boldsymbol{R}_{r,k}\tilde{\boldsymbol{\Theta}}^{\mathrm{H}}\boldsymbol{H}^{\mathrm{H}}] = \frac{\eta^2}{\sum_{i=1}^{K}\rho_i\mathrm{E}(\|\boldsymbol{h}_{r,i}\|^2)}\Bigg(\sum_{i=1}^{K}\rho_i\mathrm{E}[\bar{\boldsymbol{H}}((\boldsymbol{R}_{r,i}-\bar{\boldsymbol{h}}_{r,i}\bar{\boldsymbol{h}}_{r,i}^{\mathrm{H}})\odot\boldsymbol{R}_{r,k})\bar{\boldsymbol{H}}^{\mathrm{H}}]$$

$$+\sum_{i=1}^{K}\rho_i \mathrm{E}[\tilde{\boldsymbol{H}}((\boldsymbol{R}_{r,i}-\bar{\boldsymbol{h}}_{r,i}\bar{\boldsymbol{h}}_{r,i}^{\mathrm{H}})\odot\boldsymbol{R}_{r,k})\tilde{\boldsymbol{H}}^{\mathrm{H}}]\Big)$$
$$= \frac{\eta^2}{\sum_{i=1}^{K}\rho_i \mathrm{tr}(\boldsymbol{R}_{r,i})}\Big(\bar{\boldsymbol{H}}((\boldsymbol{R}_{r,i}-\bar{\boldsymbol{h}}_{r,i}\bar{\boldsymbol{h}}_{r,i}^{\mathrm{H}})\odot\boldsymbol{R}_{r,k})\bar{\boldsymbol{H}}^{\mathrm{H}}$$
$$+\sum_{i=1}^{K}\rho_i\sigma_\alpha^2\boldsymbol{A}_r\mathrm{diag}(\boldsymbol{A}_t^{\mathrm{H}}((\boldsymbol{R}_{r,i}-\bar{\boldsymbol{h}}_{r,i}\bar{\boldsymbol{h}}_{r,i}^{\mathrm{H}})\odot\boldsymbol{R}_{r,k})\boldsymbol{A}_t)\boldsymbol{A}_r^{\mathrm{H}}\Big). \tag{C6}$$

Combining (C2)–(C6), we can obtain the autocorrelation matrix $\boldsymbol{R}_{r,k}$ as

$$\begin{aligned}\boldsymbol{R}_{r,k} =\ & \bar{\boldsymbol{H}}\bar{\boldsymbol{\Theta}}\boldsymbol{R}_{r,k}\bar{\boldsymbol{\Theta}}^{\mathrm{H}}\bar{\boldsymbol{H}}^{\mathrm{H}}+\sigma_\alpha^2\boldsymbol{A}_r\mathrm{diag}(\boldsymbol{A}_t^{\mathrm{H}}\bar{\boldsymbol{\Theta}}\boldsymbol{R}_{r,k}\bar{\boldsymbol{\Theta}}^{\mathrm{H}}\boldsymbol{A}_t)\boldsymbol{A}_r^{\mathrm{H}}\\
&+2\mathrm{Re}\Big\{\frac{\eta\sqrt{\rho_k}}{\sqrt{\sum_{i=1}^{K}\rho_i\mathrm{tr}(\boldsymbol{R}_{r,i})}}(\bar{\boldsymbol{H}}\bar{\boldsymbol{\Theta}}\bar{\boldsymbol{h}}_{r,k}\mathrm{vec}(\mathrm{diag}(\boldsymbol{R}_{r,k}-\bar{\boldsymbol{h}}_{r,k}\bar{\boldsymbol{h}}_{r,k}^{\mathrm{H}}))^{\mathrm{T}}\bar{\boldsymbol{H}}^{\mathrm{H}}\\
&+\sigma_\alpha^2\boldsymbol{A}_r\mathrm{diag}(\boldsymbol{A}_t^{\mathrm{H}}\bar{\boldsymbol{\Theta}}\bar{\boldsymbol{h}}_{r,k}\mathrm{vec}(\mathrm{diag}(\boldsymbol{R}_{r,k}-\bar{\boldsymbol{h}}_{r,k}\bar{\boldsymbol{h}}_{r,k}^{\mathrm{H}}))^{\mathrm{T}}\boldsymbol{A}_t)\boldsymbol{A}_r^{\mathrm{H}}\\
&+\bar{\boldsymbol{H}}\bar{\boldsymbol{\Theta}}(\boldsymbol{R}_{r,k}-\bar{\boldsymbol{h}}_{r,k}\bar{\boldsymbol{h}}_{r,k}^{\mathrm{H}})\mathrm{diag}(\bar{\boldsymbol{h}}_{r,k}^{\mathrm{H}})\bar{\boldsymbol{H}}^{\mathrm{H}}\\
&+\sigma_\alpha^2\boldsymbol{A}_r\mathrm{diag}(\boldsymbol{A}_t^{\mathrm{H}}\bar{\boldsymbol{\Theta}}(\boldsymbol{R}_{r,k}-\bar{\boldsymbol{h}}_{r,k}\bar{\boldsymbol{h}}_{r,k}^{\mathrm{H}})\mathrm{diag}(\bar{\boldsymbol{h}}_{r,k}^{\mathrm{H}})\boldsymbol{A}_t)\boldsymbol{A}_r^{\mathrm{H}})\Big\}\\
&+\frac{\eta^2}{\sum_{i=1}^{K}\rho_i\mathrm{tr}(\boldsymbol{R}_{r,i})}\Big(\bar{\boldsymbol{H}}((\boldsymbol{R}_{r,i}-\bar{\boldsymbol{h}}_{r,i}\bar{\boldsymbol{h}}_{r,i}^{\mathrm{H}})\odot\boldsymbol{R}_{r,k})\bar{\boldsymbol{H}}^{\mathrm{H}}\\
&+\sum_{i=1}^{K}\rho_i\sigma_\alpha^2\boldsymbol{A}_r\mathrm{diag}(\boldsymbol{A}_t^{\mathrm{H}}((\boldsymbol{R}_{r,i}-\bar{\boldsymbol{h}}_{r,i}\bar{\boldsymbol{h}}_{r,i}^{\mathrm{H}})\odot\boldsymbol{R}_{r,k})\boldsymbol{A}_t)\boldsymbol{A}_r^{\mathrm{H}}\Big).\end{aligned} \tag{C7}$$

Then, we start to compute the expectation term $\mathrm{E}[\|\boldsymbol{\Gamma}_k^{\mathrm{H}}\boldsymbol{h}_k\|^2]$:

$$\mathrm{E}[\|\boldsymbol{\Gamma}_k^{\mathrm{H}}\boldsymbol{h}_k\|^2]=\mathrm{E}[\|\boldsymbol{h}_k^{\mathrm{H}}\boldsymbol{\Gamma}_k\boldsymbol{\Gamma}_k^{\mathrm{H}}\boldsymbol{h}_k\|]=\mathrm{tr}(\boldsymbol{R}_k\boldsymbol{R}_k^{\mathrm{sub}}) \tag{C8}$$

with

$$\boldsymbol{R}_k^{\mathrm{sub}}=\begin{bmatrix}\dfrac{\boldsymbol{R}_{1,k}}{\mathrm{tr}(\boldsymbol{R}_{1,k})} & \cdots & \boldsymbol{0}\\ \vdots & \ddots & \vdots\\ \boldsymbol{0} & \cdots & \dfrac{\boldsymbol{R}_{N_s,k}}{\mathrm{tr}(\boldsymbol{R}_{N_s,k})}\end{bmatrix}. \tag{C9}$$

As for the term $\mathrm{E}[(\boldsymbol{\Gamma}_k^{\mathrm{H}}\boldsymbol{h}_k)^{\mathrm{H}}\boldsymbol{\Gamma}_{k,e}^{\mathrm{H}}\boldsymbol{h}_k]$, we have

$$\mathrm{E}[(\boldsymbol{\Gamma}_k^{\mathrm{H}}\boldsymbol{h}_k)^{\mathrm{H}}\boldsymbol{\Gamma}_{k,e}^{\mathrm{H}}\boldsymbol{h}_k]=\mathrm{E}[\boldsymbol{h}_k^{\mathrm{H}}\boldsymbol{\Gamma}_k\boldsymbol{\Gamma}_{k,e}^{\mathrm{H}}\boldsymbol{h}_k]=\mathrm{e}^{-\frac{\sigma_\nu^2}{2}}\mathrm{E}[\mathrm{tr}(\boldsymbol{R}_k\boldsymbol{R}_k^{\mathrm{sub}})]. \tag{C10}$$

Eq. (C10) holds true because the analog precoding error $\boldsymbol{\Delta}$ is statistically independent of CSI. According to the previous work[2)], we have

$$\mathrm{E}[\mu_{m,n}\mathrm{e}^{\mathrm{j}\nu_{m,n}}]=\mathrm{e}^{-\sigma_\nu^2/2}, \tag{C11}$$

and

$$\mathrm{E}[\mu_{m,n}\mathrm{e}^{\mathrm{j}\nu_{m,n}}\mu_{i,j}^{\mathrm{H}}\mathrm{e}^{-\mathrm{j}\nu_{i,j}}]=\begin{cases}\sigma_\mu^2+1, & \forall(m,n)=(i,j),\\ \mathrm{e}^{-\sigma_\nu^2}, & \forall(m,n)\neq(i,j).\end{cases} \tag{C12}$$

Then, we focus on the expectation term $\mathrm{E}[\|(\boldsymbol{\Gamma}_k^{\mathrm{H}}\boldsymbol{h}_k)^{\mathrm{H}}\boldsymbol{\Gamma}_{k,e}^{\mathrm{H}}\boldsymbol{h}_k\|^2]$. Note that the number of antennas at the BS will be sufficiently large in THz multiuser massive MIMO systems, we apply channel hardening to $\mathrm{E}[\|(\boldsymbol{\Gamma}_k^{\mathrm{H}}\boldsymbol{h}_k)^{\mathrm{H}}\boldsymbol{\Gamma}_{k,e}^{\mathrm{H}}\boldsymbol{h}_k\|^2]$ and we can obtain

$$\mathrm{E}[\|(\boldsymbol{\Gamma}_k^{\mathrm{H}}\boldsymbol{h}_k)^{\mathrm{H}}\boldsymbol{\Gamma}_{k,e}^{\mathrm{H}}\boldsymbol{h}_k\|^2]=\mathrm{E}|\mathrm{tr}(\boldsymbol{R}_k\boldsymbol{R}_k^{\mathrm{sub}}\boldsymbol{\Delta}^{\mathrm{H}})|^2=\mathrm{e}^{-\sigma_\nu^2}|\mathrm{tr}(\boldsymbol{R}_k\boldsymbol{R}_k^{\mathrm{sub}})|^2. \tag{C13}$$

Similarly, we can compute the term $\mathrm{E}[\|(\boldsymbol{\Gamma}_k^{\mathrm{H}}\boldsymbol{h}_k)^{\mathrm{H}}\boldsymbol{\Gamma}_{k,e}^{\mathrm{H}}\boldsymbol{h}_i\|^2]$ as follows:

$$\mathrm{E}[\|(\boldsymbol{\Gamma}_k^{\mathrm{H}}\boldsymbol{h}_k)^{\mathrm{H}}\boldsymbol{\Gamma}_{k,e}^{\mathrm{H}}\boldsymbol{h}_i\|^2]=\mathrm{tr}(\boldsymbol{R}_k\boldsymbol{R}_k^{\mathrm{sub}}\boldsymbol{R}_i^e\boldsymbol{R}_k^{\mathrm{sub}}) \tag{C14}$$

with

$$(\boldsymbol{R}_i^e)_{m,n}=\begin{cases}(1+\sigma_\mu^2)(\boldsymbol{R}_i)_{m,n}, & \forall m=n,\\ \mathrm{e}^{-\sigma_\nu^2}(\boldsymbol{R}_i)_{m,n}, & \forall m\neq n.\end{cases} \tag{C15}$$

Finally, we compute the expectation term $\mathrm{E}[\|(\boldsymbol{\Gamma}_k^{\mathrm{H}}\boldsymbol{h}_k)^{\mathrm{H}}\boldsymbol{\Gamma}_{k,e}^{\mathrm{H}}\boldsymbol{n}\|^2]$ as follows:

$$\mathrm{E}[\|(\boldsymbol{\Gamma}_k^{\mathrm{H}}\boldsymbol{h}_k)^{\mathrm{H}}\boldsymbol{\Gamma}_{k,e}^{\mathrm{H}}\boldsymbol{n}\|^2]=\sigma_u^2\mathrm{E}[\boldsymbol{h}_k^{\mathrm{H}}\boldsymbol{\Gamma}_k\boldsymbol{\Gamma}_{k,e}^{\mathrm{H}}\boldsymbol{\Gamma}_{k,e}\boldsymbol{\Gamma}_k^{\mathrm{H}}\boldsymbol{h}_k]=\sigma_u^2(\sigma_\mu^2+1)\mathrm{tr}(\boldsymbol{R}_k\boldsymbol{R}_k^{\mathrm{sub}}\boldsymbol{R}_k^{\mathrm{sub}}). \tag{C16}$$

2) Wang W J, Liu A, Zhang Q, et al. Robust multigroup multicast transmission for frame-based multi-beam satellite systems. IEEE Access, 2018, 6: 46074–46083